ANNALS OF GEOPHYSICS, 59, FAST TRACK 5, 2016; DOI: 10.4401/ag-7246

The first month of the 2016 central Italy seismic sequence: fast determination of time domain moment tensors and finite fault model analysis of the M_L 5.4 aftershock

LAURA SCOGNAMIGLIO*, ELISA TINTI, MATTEO QUINTILIANI

Istituto Nazionale di Geofisica e Vulcanologia

*laura.scognamiglio@ingv.it

Abstract

*We present the revised Time Domain Moment Tensor (TDMT) catalogue for earthquakes with M_L larger than 3.6 of the **first month of the** ongoing Amatrice seismic sequence **(August 24th - September 25th)**. Most of the retrieved focal mechanisms show NNW–SSE striking normal faults in agreement with the main NE-SW extensional deformation of Central Apennines. We also report a preliminary finite fault model analysis performed on the larger aftershock of th**is period of the** sequence (M_w 5.4) and discuss the obtained results in the framework of aftershocks distribution.*

I. INTRODUCTION

The M_L 6.0 Amatrice earthquake, which occurred at 01:36:32 UTC August 24th 2016 is the first mainshock of the Amatrice seismic sequence. It is the largest earthquake to strike this portion of central Apennines since the *M* 6.2, 1639 October 7th Monti della Laga Earthquake archived as an *I*=IX-X (MCS) and *M*=6.2, [CPTI15, Rovida et al., 2016]. The earthquake caused **299** fatalities and partially destroyed the towns of Amatrice, Accumoli and several surrounding small towns. The hypocenter is located at 42.70° N, 13.23° E and at depth of 8km, only 1 km far from the Accumoli village and just 9 km from the Amatrice town [Marchetti et al., *this issue*]. Almost one hour after the mainshock, an aftershock of M_L 5.4 occurred; it is located 12 km NW of the mainshock close to the Norcia town. No significant foreshocks were recorded.

Soon after the mainshock evidence for 5.2 km of surface ruptures, preliminarily interpreted as a direct expression of coseismic fault rupture, was observed along the northwest-striking Mt. Vettore fault trace by Emergeo Working Group geologists [EMERGEO W. G., *this issue*] (Figure 1). The average surface offsets found is in the order of 15-20 cm for both heave and throw components.

The kinematic finite fault model, retrieved starting from the TDMT mainshock solution, shows that the Amatrice earthquake ruptured a fault dimension 26 km long and 16 km width [Tinti et al., 2016]. The most relevant features of this model are (i) clear bilateral rupture, (ii) rela-

tively fast rupture velocity, (iii) heterogeneity of the slip distribution characterized by two main slip patches and iv) quite different value of the rake on the two patches [Tinti et al., 2016]. The rupture from this normal fault earthquake propagates bilaterally to SE and to N-NW directing the strongest shaking toward the city of Amatrice, where peak ground accelerations (PGAs) between 19%*g* and 43%*g* is recorded, and toward the town of Norcia, where PGAs ranges between 22%*g* and 37%*g* [Faenza et al., *this issue*].

The preliminary aftershocks distribution defines a main fault plane SW-dipping with an average dip angle of ~50° in agreement with the computed moment tensor solution. The main fault plane is simpler to the south while it becomes more complex to the northernmost portion where it is evident the activation of a shallower and antithetic splay. The aftershocks distribution suggests an along strike fault length of about 35 km [Michele et al., *this issue*].

Here, we report on source geometries of the, still active, Amatrice seismic sequence relatively to the period of time spanning from August 24thto September 25th. We present the revised moment tensor solutions of all the events with M_L > 3.3. Due to the complex aftershocks distribution on the northern part of the seismic sequence, we decided to try to understand the larger aftershock of the sequence with the aim of identifying which is the activated fault plane and the main characteristic of the rupture. We believe that understanding the main features of this first period of the Amatrice seismic sequence could contribute to explain the complexity of the seismogenic processes active in the Central Apennines that has been marked by three mainshocks in two months of moment magnitude 6.0, 5.9 and 6.5 respectively (http://cnt.rm.ingv.it/en/tdmt).

II. Seismic sequence moment Tensor Solutions

Moment tensor solution presented in this study are computed by following the full-waveform TDMT technique originally proposed by Dreger & Helmberger (1993) and implemented in an automatic-way at INGV by Scognamiglio *et al*. (2009). Starting from a given hypocentral location, the algorithm inverts local to regional three component broad-band velocity waveforms to estimate moment tensor in a point-source approximation. We adopt the pre-calculated and stored Green's functions obtained using the CIA (Central Italian Apennines) velocity model [Herrmann et al., 2011] that has been inferred for the central Apennines during the 2009 L'Aquila sequence. Quality and reliability of moment tensors are based on the goodness of fit between synthetic and observed waveforms, which is quantified through the variance reduction (VR) parameter, that represents an L2-like norm [Scognamiglio et al., 2010]. For events in the magnitude M_L 3.8 and larger range we have found that an appropriate filter is low-pass at 0.05 Hz followed by a high-pass filter of 0.02 Hz. Lower magnitude earthquakes were inverted in the frequency band of 0.02-0.1Hz.

We have revised TDMT solutions for 64 events of the first month of the Amatrice seismic sequence including all the events with M_L larger **than 3.2 for** which we were able to obtain a well-constrained solution (Figure 1 and Table 1). Comparing definitive to automatic solutions, computed immediately after the earthquakes, we found really smaller adjustments to quick determinations. This highlights the robustness of the methodology adopted and the appropriate choice of the velocity model, that allows us to reach for this sequence a magnitude lower threshold equal to M_w 3.2. Most of these solutions have 'Aa' quality flag, that means very good fit between data and synthetics and high double-couple value (http://cnt.rm.ingv.it/en/help#TDMT). Centroid depth of all solutions is between 1 and 8 km, in most cases shallower than the INGV released locations [Marchetti et al., *this issue*].

The 01:36 mainshock moment tensor solution, obtained inverting 50 stations in a distance range is of ~65-260 km, shows normal faulting with

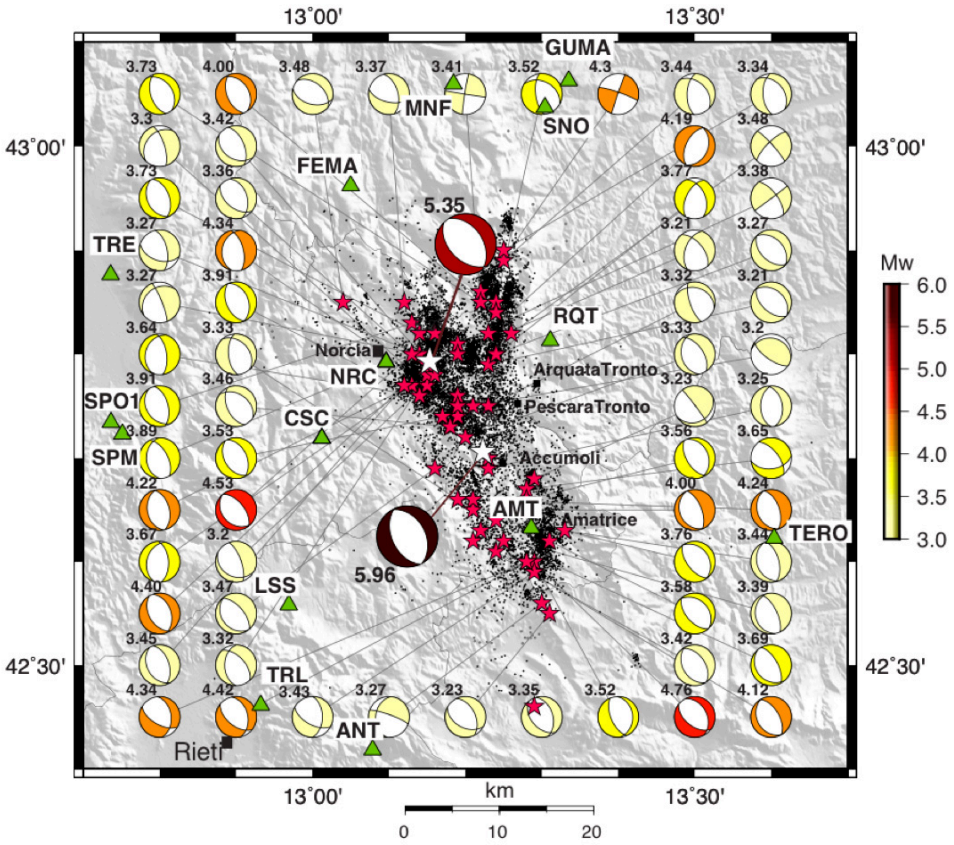

Figure 1. *Map view of TDMT solutions of the **first month of the** Amatrice 2016 seismic sequence. Beach Balls are colored as a function of magnitude that is also reported on top of each mechanism. White stars are mainshock and biggest aftershock location. Red stars are the focal mechanism location. Black dots are the Michele et al. [this issue] relocated aftershocks. Green triangles are the strong motion stations used for the finite fault analysis.*

nodal planes striking along the Apenninic direction equal to strike 155°/331°, dip 49°/41° and rake −85°/-93°. The estimated scalar seismic moment is 1.07 10^{+18} N·m for a preferred centroid depth of 5 km, corresponding to a moment magnitude of M_w 5.96. The M_L 5.4 biggest aftershock, which occurred at 02:33:29 UTC 24 August 2016, also features a normal fault mechanism, the obtained focal parameters are strike 135°/327°, dip 47°/43°, and rake –98°/-81°. The solution is calculated using 62 stations in the distance range of 51-130 km. The preferred centroid depth is 5 km, while the seismic moment is 1.33 10^{+17} N·m resulting in a M_w 5.4. With the exception of the mainshock, this is the only earthquake of the first month of the sequence with M_w larger than 5.

The remaining **62** moment tensor solutions shows that NNW–SSE striking normal faults dominate, which is in overall agreement with the trends of structures of this sector of Central Apennines. Only in a few cases, a strike-slip kinematic characterizes the source geometry of the obtained MT, as for the August 31, 11:52 and 18:12 (UTC) aftershocks, with magnitude M_w 3.4 and 3.5 respectively, and for the September 3, 10:19 (UTC) M_w 4.3. These events are all located in

the northern portion of the area activated by this first month of the sequence, the same area that would have been affected by the other two mainshocks of 26th October, M_w 5.9, and 30th October, M_w 6.5. The complete information and the fit to recorded waveforms are available on the dedicated webpage (http://cnt.rm.ingv.it/en/tdmt), where automatic good quality solutions of smaller events are also available.

Date	Origin Time	Longitude	Latitude	Depth	Strike 1	Dip 1	Rake 1	Strike 2	Dip 2	Rake 2	M_w
2016-08-24	01:36:32	13.23	42.7	5	155	49	-87	331	41	-93	5.96
2016-08-24	01:56:00	13.28	42.6	2	120	60	-123	353	43	-47	4.34
2016-08-24	02:33:28	13.15	42.79	5	135	47	-98	327	43	-81	5.35
2016-08-24	02:59:35	13.13	42.8	5	332	58	-105	179	35	-67	3.89
2016-08-24	03:08:10	13.25	42.62	5	331	64	-85	139	26	-101	3.69
2016-08-24	03:17:59	13.14	42.76	5	351	62	-104	198	31	-66	3.64
2016-08-24	03:40:10	13.24	42.61	6	329	59	-90	150	31	-89	4.12
2016-08-24	04:06:50	13.12	42.77	3	149	47	-97	340	44	-82	4.40
2016-08-24	04:25:58	13.24	42.64	6	345	59	-87	159	31	-96	3.44
2016-08-24	04:33:09	13.21	42.62	5	325	49	-93	149	41	-87	3.42
2016-08-24	04:38:09	13.22	42.63	6	334	67	-96	169	23	-76	3.39
2016-08-24	04:44:38	13.18	42.73	6	155	54	-71	305	40	-114	3.46
2016-08-24	04:57:37	13.04	42.85	2	105	48	-109	311	45	-71	3.48
2016-08-24	05:02:24	13.29	42.46	7	139	47	-107	343	45	-72	3.35
2016-08-24	05:31:32	13.19	42.66	6	175	59	-69	318	37	-122	3.33
2016-08-24	05:36:19	13.14	42.8	7	338	81	-117	231	29	-19	3.27
2016-08-24	06:54:54	13.19	42.8	6	320	58	-134	201	52	-42	3.21
2016-08-24	07:10:55	13.16	42.78	5	340	70	-71	116	27	-131	3.2
2016-08-24	09:31:43	13.19	42.81	12	53	89	24	323	66	179	3.38
2016-08-24	11:50:30	13.16	42.82	6	321	59	-88	137	31	-94	4.53
2016-08-24	14:02:20	13.24	42.8	3	207	56	-55	336	47	-130	3.77
2016-08-24	17:46:09	13.21	42.66	7	340	57	-89	158	33	-91	4.24
2016-08-24	20:21:36	13.15	42.78	5	317	56	-117	180	43	-56	3.32
2016-08-24	23:22:05	13.21	42.65	6	338	63	-89	156	27	-91	4.00
2016-08-25	03:17:16	13.19	42.75	6	345	61	-105	193	32	-65	4.34
2016-08-25	04:12:11	13.23	42.69	5	180	47	-84	350	44	-97	3.25
2016-08-25	04:51:40	13.33	42.63	2	143	60	-91	325	30	-88	3.76
2016-08-25	12:36:05	13.28	42.6	5	129	55	-115	347	42	-60	4.42
2016-08-25	19:40:44	13.29	42.59	5	119	59	-132	360	50	-41	3.43
2016-08-26	00:04:09	13.28	42.66	3	149	58	-95	338	33	-82	3.56
2016-08-26	04:28:25	13.29	42.6	5	128	53	-106	333	40	-70	4.76
2016-08-26	05:17:05	13.21	42.75	7	125	69	98	283	22	70	3.20
2016-08-26	05:32:52	13.15	42.77	6	342	71	-119	222	34	-35	3.30
2016-08-26	16:05:29	13.16	42.69	6	319	62	-92	143	28	-86	3.47
2016-08-27	01:26:39	13.24	42.84	2	162	54	-79	324	37	-105	3.73
2016-08-27	02:50:59	13.24	42.84	3	158	53	-83	327	38	-99	4.00
2016-08-27	06:20:30	13.31	42.55	3	334	50	-65	118	46	-117	3.23
2016-08-27	10:40:14	13.24	42.85	2	173	65	-60	299	39	-137	3.52
2016-08-28	06:37:19	13.2	42.72	7	326	56	-102	166	35	-73	3.33

2016-08-28	13:07:32	13.29	42.6	6	156	61	-100	356	30	-72	3.52
2016-08-28	15:37:38	13.12	42.77	6	342	52	-83	150	39	-99	3.45
2016-08-28	15:55:35	13.23	42.82	5	206	55	-87	22	35	-94	4.19
2016-08-28	16:42:01	13.14	42.82	5	340	51	-86	154	39	-95	3.73
2016-08-29	01:44:25	13.19	42.76	7	129	50	-113	342	45	-66	3.36
2016-08-30	00:35:55	13.14	42.8	6	347	60	-51	108	48	-137	3.27
2016-08-31	11:26:01	13.13	42.83	5	345	56	-80	147	35	-105	3.91
2016-08-31	11:52:31	13.22	42.85	4	99	89	177	189	87	1	3.41
2016-08-31	13:23:04	13.23	42.75	6	161	71	-67	288	29	-140	3.32
2016-08-31	18:12:52	13.26	42.82	7	318	83	-164	225	74	-8	3.48
2016-09-01	03:53:04	13.31	42.62	5	139	57	-88	315	33	-93	3.58
2016-09-01	11:35:57	13.3	42.56	5	290	81	-124	186	35	-17	3.27
2016-09-03	01:34:12	13.13	42.77	4	345	51	-92	169	39	-87	4.22
2016-09-03	10:18:51	13.22	42.86	8	199	88	-7	289	83	-178	4.30
2016-09-07	18:13:26	13.24	42.8	1	134	49	-91	315	41	-89	3.27
2016-09-15	14:40:52	13.13	42.77	2	356	54	-102	196	37	-74	3.67
2016-09-19	23:34:25	13.28	42.67	4	322	61	-52	83	46	-138	3.65
2016-09-20	01:20:53	13.29	42.68	6	323	87	-68	59	23	-173	3.23
2016-09-22	20:03:55	13.19	42.76	5	337	58	-71	123	37	-118	3.42
2016-09-30	19:22:28	13.25	42.9	5	177	57	-67	318	39	-122	3.34
2016-09-30	19:38:37	13.25	42.89	5	182	59	-61	315	41	-129	3.44
2016-10-02	23:47:07	13.23	42.79	2	133	53	-88	309	37	-93	3.21
2016-10-04	12:41:35	13.12	42.85	5	103	57	-136	345	54	-42	3.37
2016-10-08	12:19:03	13.17	42.74	3	334	47	-86	148	43	-94	3.53
2016-10-08	18:11:09	13.19	42.74	2	156	51	-91	338	39	-88	3.91

Table 1. *Moment tensor solutions obtained using the TDMT technique. The complete information and the fit to recorded waveforms are available on the dedicated web-page (http://cnt.rm.ingv.it/en/tdmt).*

III. ANALYSIS OF THE M_w 5.4 AFTERSHOCK FAULT PLANE

One hour after the 24th August mainshock, a Mw 5.4 event occurred almost 12 km NW from the mainshock. TDMT procedure reveals a normal faulting moment tensor solution having strike directions diverging from the mainshock fault rupture of ~20° for the west-dipping plane and ~4° for the east-dipping plane. This is the biggest aftershock of the sequence, the only one with magnitude larger than 5. It is located in the northern portion of the region activated by the Amatrice seismic sequence, ~5 km far from Norcia town.

To unravel the ambiguity on what fault plane actually ruptured, we perform a series of inversions using waveform data recorded by 15 strong-motion INGV [Michelini et al., 2016] and RAN (http://ran.protezionecivile.it/ET/index.php) stations, and adopting the TDMT source geometry (strike and dip) on an overly-large-dimension fault plane centered on the NLL relocated hypocenter: latitude 42.793° N, longitude 13.162° E and depth 6.835 km [Michele et al., *this issue*]. The epicentral distances of the selected recording sites are less than 45 km We use the inversion code based on the method of Hartzell and Heaton [1983], and implemented by Dreger et al. [2005] consisting in a non-negative, least-squares inversion method with simultaneous smoothing and damping, the same used to infer the source parameters of the mainshock.

This approach assumes a constant rupture velocity and rise time and the best fitting values have been selected iteratively by performing

inversions with different values of these parameters and quantitatively measuring the fit based on a variance reduction, as defined above for TDMT solutions [Scognamiglio et al., 2010]. Rake parameter can be heterogeneous on the fault plane or assumed constant all over the fault and chosen iteratively as the rupture velocity.

The slip velocity is modeled by imposing a simple box-car source-time function. The Green's functions are computed on a regular grid sampling the focal volume every 1 km horizontally and 1 km vertically and filtered between 0.02 and 0.5 Hz, the same as for the recorded data. The velocity structure is CIA model [Herrmann et al., 2011], the same adopted for TDMT solutions. We are aware that the maximum selected frequency could prevent us to identify the details of the rupture history for a M 5 earthquake, but it allows us to reduce the impact of site effects like those reported for Norcia station (NRC) for higher frequencies [Bindi et al., 2011]. We run more than 1000 inversions for both planes by setting rise time and rupture velocity ranging between 0.3 ÷ 1 s and 2.0 ÷ 4 km/s respectively, while rake is allowed to vary in a 30°-long range respect to the TDMT values. The faults are parameterized using subfaults having a 2 x 2 km^2 area. The overly-large modeled fault planes are 10 km x 10km. Figure 2(a, b) shows the resulting preferred slip models for both the inverted planes and the corresponding waveforms fit.

The east-dipping plane displays a main slip concentration located ~4 km southeastward from the hypocenter at similar depth. This patch accounts for a maximum slip of about 20 cm. The picked rise time is 0.3 s, the rupture velocity is 2.7 km/s, and the rake is -91°. The total inferred seismic moment is 9.78 10^{16} Nm corresponding to M_w = 5.29. The west-dipping plane features two slip patches both located 2 km deeper than the hypocenter. The first asperity is located just below the nucleation and has average slip equal to 16 cm, the second one is located ~ 4 km SE and reports a maximum slip of 22 cm. The retrieved rise time is 0.3 s, while the rupture velocity is 3.7 km/s and the rake -115°. The total inferred seismic moment is 9.53 10^{16} Nm corresponding to M_w = 5.29.

Both the inverted rupture planes prefer the shortest rise time that, for the inverted frequencies, means to consider a delta-like slip velocity function. Otherwise, while the preferred rupture velocity for the N327° plane finds a clear maximum within the explored rupture velocities, the high value found for the N135° plane cannot be considered well-constrained due to a very similar variance reduction (~30%) we obtain for rupture velocities between 3.0 and 3.9 km/s (Figure 3a). Although we adopt an overly-large fault plane to image the model parameters, significant slip occurs only on an area of 8 x 5 km^2. The comparison between recorded and synthetic data retrieved from the two rupture models is presented in Figure 2c. The synthetic ground velocities generated by the N327° slip model match fairly well the main body wave pulses of the majority of the recorded seismograms. On the contrary, the rupture model obtained for the west-dipping plane poorly fits the main features of real data except for the three farthest stations and NRC.

Both models show discrepancies at some sites most likely resulting from 3D variations of velocity structure in this area not included in our adopted 1D velocity model [Casarotti et al., *this issue*]. As an example, stations located in the northern side show a poor fit (e.g. FEMA) and would require a faster velocity structure to allow a better alignment between real and synthetic phases.

Figure 3b shows the evolution of the VR values for the performed inversions with rise time equal to 0.3s. Among all the performed inversions, we have found more than 60% of the solutions adopting the east-dipping plane having VR larger than 30% with an overall VR_{MAX}= 35%, while, for the alternative west-dipping plane, only 13% feature VR larger than 30% with an overall VR_{MAX}= 31%. The finite fault inversion result opts for the activation of the strike 327° fault plane. However, the small dif-

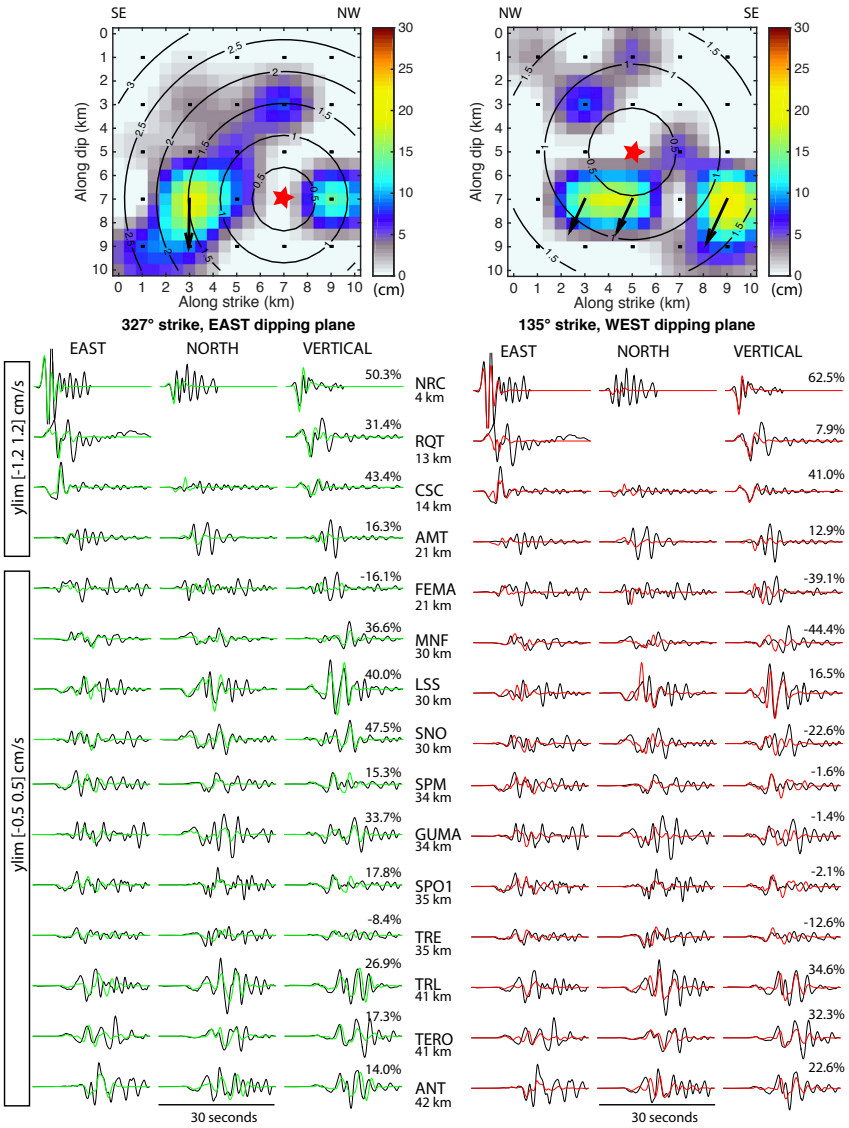

Figure 2. *Rupture models imaged by inverting ground velocity time histories for the* ***(a)*** *east dipping plane (N327°) and* ***(b)*** *west dipping plane (N135°) respectively. The black arrows indicate the slip direction (rake angle) for slip larger than 15 cm.* ***(c)*** *Fit to the data: synthetic ground velocity filtered between 0.02 and 0.5 Hz (green and red lines are for the east and west dipping planes respectively) and recorded strong motions (black lines). Numbers in box represent the amplitude range in cm/s. Numbers in percentage represent the Variance Reduction for each station.*

ference between the resulting VR_{MAX} values do not allow us to exclude a priori the activation of the strike 135° fault.

To solve the ambiguity of the kinematic result we decide to analyze the aftershocks distribution and verify the existence of earthquakes align-

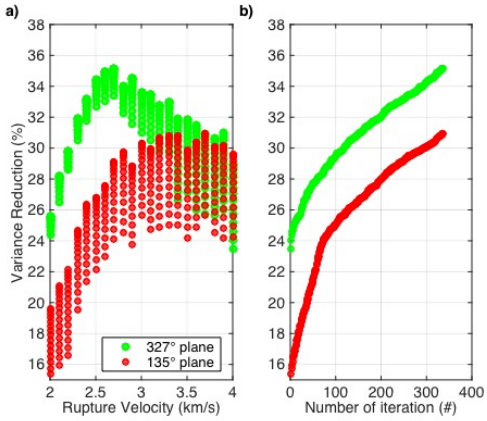

Figure 3 (above). *Resulting variance reduction for a subset of 336 inversions performed with rise-time equal to 0.3s. Rupture velocity and rake angle vary within the explored range. Green dots are for the striking N327° plane while red dots are for the striking N135°plane.* ***(a)*** *VR is shown as a function of rupture velocity;* ***(b)*** *VR is sorted for increasing values. The variability of VR for each rupture velocity (panel a) reflects the variability in rake.*

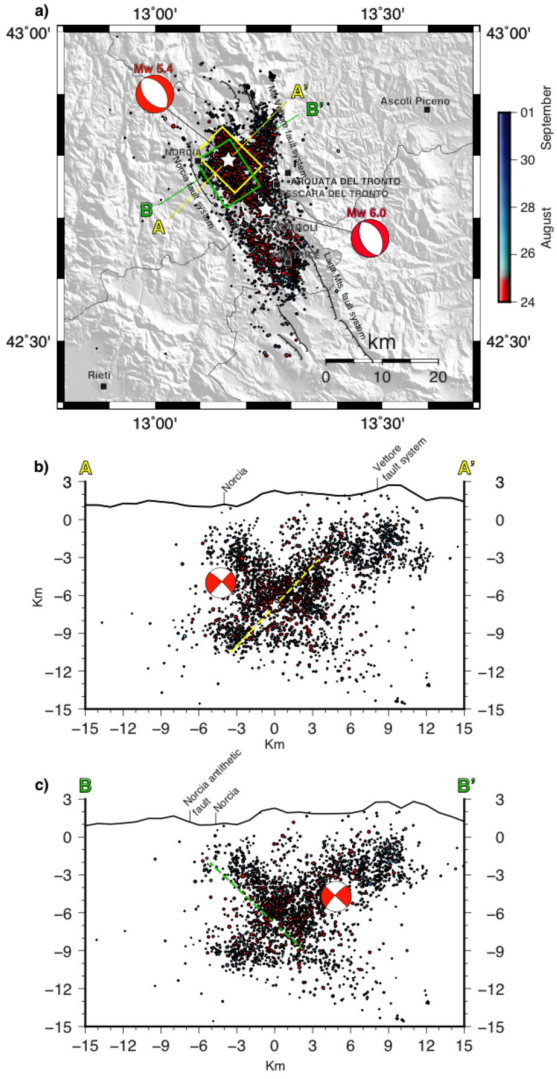

Figure 4 (right column). ***(a)*** *Map view of the relocated aftershocks [Michele et al., this issue] with traces of the active mapped faults [EMERGEO W. G., this issue]. White stars represent the location of the largest events of the* ***studied*** *sequence. Earthquakes are colored as a function of date of occurrence. Yellow and green boxes are the map projection of the inverted fault while the yellow and green lines correspond to the vertical sections reported in panels* ***(b)*** *and* ***(c)*** *showing the earthquakes occurring within 8km from the vertical line.*

ment on the investigated rupture planes. We plot the first 8 days of the aftershocks sequence relocated by Michele et al. [*this issue*] along two vertical sections oriented N45°E and N57°E, perpendicular to the strike of the TDMT planes (Figure 4). Due to the not completely 100% double couple component of the moment tensor solution, the profiles are rotated 12° from each other. Aftershocks are shown with dots colored as function of date of occurrence. Each section reports earthquakes occurring in the 8 x 15 km^2 boxes mapped in Figure 4a and the trace of the inverted fault planes, as well as the mapped main normal fault systems [EMERGEO W. G., *this issue*].

At first glance, both profiles show a cross-like events distribution that reveals the activation in this area of both synthetic and antithetic

structures. In the N45°E oriented A-A' profile, the seismicity does not clearly image a continuous single west-dipping plane, but it is quite diffuse and probably related to the NW termination of the fault activated during the mainshock [Tinti et al., 2016, Michele et al., *this issue*]. On the contrary, along the B-B' section, the distribution of the aftershocks along the dip of the inverted N327° rupture plane is irregular but in some way more evident. For this plane we also find a quite good geometrical correspondence with the mapped Norcia antithetic fault.
Both the vertical sections also image a separated hypocenters cluster below the Mt. Vettore fault system.

IV. Conclusion

In this paper we have presented the revised TDMT catalogue for all the events with M_L larger than 3.**2** belonging to the first month if the 2016 Amatrice (Central Italy) seismic sequence. The moment tensor solutions immediately pointed up a prevalent normal faulting mechanism for the occurring earthquakes, in agreement with the present-day active stress field in this sector of the Apennines. Only in a few cases, mainly located in the northern portion of the area activated by the seismic sequence, a strike-slip kinematic characterizes the source geometry. Centroid depths are between 1 and 8 km, typically shallower than the INGV released location [Marchetti et al., *this issue*].
We have found a really good agreement between revised and automatic solutions, computed immediately after the earthquakes occurrence, confirming once again the implemented method as a robust and practical tool for real-time determinations of the point-source focal parameters and magnitude.
We have analyzed the largest aftershock of the first month of the sequence (M_w 5.4) in terms of finite rupture model with the aim of identifying the activated fault plane. We have performed more than 1000 inversions to model both the fault plane geometries identified by TDMT solution and we have found a quite satisfactory fit by using strong motion data at epicentral distance less than 45 km and frequencies up to 0.5 Hz. The finite fault inversion results opt for the activation of the strike N327° fault plane. The small difference of variance reduction between the two best solutions does not allows us to exclude a priori the activation of the strike 135° fault. In any case, both the models reveal, as a common feature, a main asperity located south-east from the hypocenter characterized by a maximum slip of ~ 20 cm.
To give an additional constraint to the kinematic result we have decided to analyze the first 8 days of aftershocks distribution and verify the existence of earthquakes alignment on the investigated rupture planes.
The preliminary analysis of finite fault model and aftershocks distribution suggests that, for the M_w5.4 aftershock, the most probably activated fault plane is the one striking N327°and dipping 43° toward NE. For this plane we find a quite good geometrical correspondence with the mapped Norcia antithetic fault.

References

[Bindi et al., 2011] Bindi, D., L. Luzi, S. Parolai, D. Di Giacomo, and G. Monachesi (2011). Site effects observed in alluvial basins: the case of Norcia (Central Italy), Bulletin of Earthquake Engineering, 9(6), 1941-1959, doi:10.1007/s10518-011-9273-3.

[Dreger et al., 2005] Dreger, D. S., L. Gee, P. Lombard, M. H. Murray, and B. Romanowicz (2005). Rapid finite-source analysis and near-fault strong ground motions: Application to the 2003 Mw 6.5 San Simeon and 2004 Mw 6.0 Parkfield earthquakes, *Seismological Research Letters 76 (1)*, 40-48.

[EMERGEO W. G., *this issue*] Emergeo Working Group (2016). Coseismic effects of the 2016 Amatrice seismic sequence: first geological results. Annals of Geophysics, this issue.

[Faenza et al., *this issue*] Faenza, L., V. Lauciani and A. Michelini (2016). The ShakeMaps of the Amatrice, M6, earthquake. Annals of Geophysics, this issue.

[Hartzell and Heaton, 1983] Hartzell, S.H., and T.H. Heaton (1983). Inversion of strong ground motion and teleseismic waveform data for the fault rupture history of the 1979 Imperial Valley, California, earthquake, Bull. Seis. Soc. Am 73 (6, Part A),1553-1583.

[Herrmann et al., 2011] Herrmann, R.B., L. Malagnini, and I. Munafò (2011). Regional moment tensor of the 2009 L'Aquila earthquake sequence, Bull.seism.Soc.Am.,101(3), 975-993.

[Marchetti et al., *this issue*] Marchetti A., M.G. Ciaccio, A. Nardi, A. Bono, F.M. Mele, L. Margheriti, A. Rossi, P. Battelli, C. Melorio, B. Castello, V. Lauciani, M. Berardi, C. Castellano, L. Arcoraci, G. Lozzi, A. Battelli, C. Thermes, N. Pagliuca, G. Modica, A. Lisi, L. Pizzino, P. Baccheschi, S. Pintore, M. Quintiliani, A. Mandiello, C. Marcocci, M. Fares, D. Cheloni, A. Frepoli, D. Latorre, A.M. Lombardi, M. Moretti, M. Pastori, M. Vallocchia, A. Govoni, L. Scognamiglio, A. Basili. A. Michelini and S. Mazza (2016). The Italian Seismic Bulletin: strategies, revised pickings and locations of the Amatrice seismic sequence, Annals of Geophysics, this issue.

[Michele et al., *this issue*] Michele M., Di Stefano R., Chiaraluce L., Cattaneo M., De Gori P., Monachesi G., Latorre D., Marzorati S., Valoroso L., Ladina C., Chiarabba C., Lauciani V. and M. Fares (2016). The Amatrice 2016 seismic sequence: a preliminary look to the mainshock and aftershocks distribution, Annals of Geophysics, this issue.

[Michelini et al., 2016] Michelini, A., Margheriti, L., Delladio, A., Pintore, S., Cecere, G., G. D'Anna, G., Moretti, M., Cattaneo, M., Marchetti, A., Demartin, M., Mazza, S., Mele, F., Lauciani, V., Bono, A., Marcocci, C., Quintiliani, M., Scognamiglio, L., Faenza, L., Amato, A., Basili, A., Selvaggi, G., Nardi, A., Danecek, P., Pignone, P., Nostro, C., Casale, P., Mandiel-lo, A. and S. Rao (2016). The Italian National Seismic Network and the earthquake and tsunami monitoring and surveillance systems, (submitted to Advances in Geosciences).

[Rovida et al., 2016] Rovida A., Locati M., Camassi R., Lolli B., Gasperini P., eds. (2016). CPTI15, the 2015 version of the Parametric Catalogue of Italian Earthquakes, Istituto Nazionale di Geofisica e Vulcanologia; doi:http://doi.org/10.6092/INGV.IT-CPTI15.

[Scognamiglio et al., 2009] Scognamiglio, L., Tinti, E. and Michelini, A. (2009). Real-time determination of seismic moment tensor for Italian Region, Bull. seism. Soc. Am., **99**(4), 2223-2242.

[Scognamiglio et al., 2010] Scognamiglio, L., E. Tinti, A. Michelini, D. S. Dreger, A. Cirella, M. Cocco, S. Mazza, and A. Piatanesi (2010). Fast determination of moment tensors and rupture History: what has been learned from the 6 April 2009 l'Aquila earthquake sequence, Seism. Res. Lett., 81(6), 892-906; doi:10.1785/gssrl.81.6.892.

[Tinti et al., 2016] Tinti, E., L. Scognamiglio, A. Michelini, and M. Cocco (2016). Slip heterogeneity and directivity of the ML 6.0, 2016, Amatrice earthquake estimated with rapid finite-fault inversion, Geophys. Res. Lett., 43, 10,745-10,752; doi:10.1002/2016GL071263.